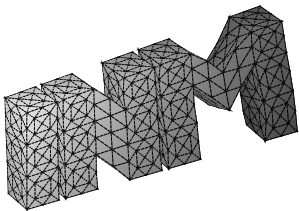

Boundary integral formulations for the forward problem
in magnetic induction tomography

S. Engleder, O. Steinbach



**Berichte aus dem
Institut für Numerische Mathematik**

Technische Universität Graz

Boundary integral formulations for the forward problem
in magnetic induction tomography

S. Engleder, O. Steinbach

**Berichte aus dem
Institut für Numerische Mathematik**

Bericht 2010/4

Technische Universität Graz
Institut für Numerische Mathematik
Steyrergasse 30
A 8010 Graz

WWW: <http://www.numerik.math.tu-graz.ac.at>

© Alle Rechte vorbehalten. Nachdruck nur mit Genehmigung des Autors.

Boundary integral formulations for the forward problem in magnetic induction tomography

S. Engleder, O. Steinbach

Institut für Numerische Mathematik, TU Graz
Steyrergasse 30, 8010 Graz, Austria

Abstract

In this paper we present two models for the forward problem of magnetic induction tomography. In particular, we describe the eddy current model, and a reduced simplified model. The error between the reduced and the full model is analysed in dependence of parameters such as the frequency and the conductivity. In the case of a piecewise constant conductivity we derive a boundary integral formulation for the reduced model. Finally we comment on numerical results for the forward problem and give a comparison of both models.

1 Introduction

Magnetic induction tomography is a non-invasive and contactless imaging method to determine the conductivity and permittivity distribution inside a certain object, like the human body, see, e.g., [6, 7, 9, 10, 16]. An array of coils is placed in a ring around the body as depicted in Fig. 1. In each coil a time-harmonic current is induced, which generates a time-harmonic magnetic field. This so-called primary magnetic field \mathbf{B}_p induces eddy

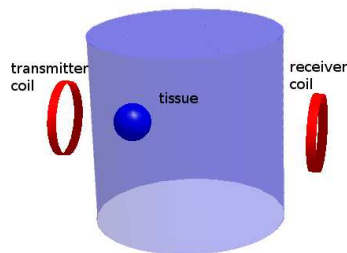


Figure 1: Principle of magnetic induction tomography.

currents inside the body, which perturb the magnetic field. The reconstruction is then

based on the measurement of the perturbed voltage in an array of receiver coils around the body.

To describe the forward problem of magnetic induction tomography we use the time-harmonic Maxwell equations for $x \in \mathbb{R}^3$,

$$\nabla \times \mathbf{E}(x) = -i\omega \mathbf{B}(x), \quad \nabla \times \mathbf{H}(x) = \mathbf{j}(x) + i\omega \mathbf{D}(x), \quad \nabla \cdot \mathbf{D}(x) = 0, \quad \nabla \cdot \mathbf{B}(x) = 0,$$

where we consider an isotropic and linear material, i.e.,

$$\mathbf{D}(x) = \varepsilon(x)\mathbf{E}(x), \quad \mathbf{B}(x) = \mu(x)\mathbf{H}(x), \quad \mathbf{j}(x) = \mathbf{j}_i(x) + \sigma(x)\mathbf{E}(x).$$

When considering biologic tissues we may assume a constant permeability $\mu(x) = \mu_0$. The coil is modelled by prescribing a given impressed current \mathbf{j}_i , of which we assume that it is not influenced by the magnetic reaction fields caused by the eddy currents inside the conducting domain. Hence we conclude

$$\nabla \times \mathbf{E}(x) = -i\omega\mu_0\mathbf{H}(x), \quad \nabla \times \mathbf{H}(x) = \mathbf{j}_i(x) + \kappa(x)\mathbf{E}(x), \quad \nabla \cdot [\varepsilon(x)\mathbf{E}(x)] = 0, \quad \nabla \cdot \mathbf{H}(x) = 0,$$

where

$$\kappa(x) := \sigma(x) + i\omega\varepsilon(x) \tag{1.1}$$

is the complex conductivity. When eliminating the magnetic field \mathbf{H} we finally obtain

$$\nabla \times \frac{1}{\mu_0} \nabla \times \mathbf{E}(x) + i\omega\kappa(x)\mathbf{E}(x) = -i\omega\mathbf{j}_i(x), \quad \nabla \cdot [\varepsilon(x)\mathbf{E}(x)] = 0 \quad \text{for } x \in \mathbb{R}^3. \tag{1.2}$$

In particular when considering the inverse problem of magnetic induction tomography, for example by using a standard parameter identification approach, the solution of the forward problem depends on the boundary mesh only. Hence it seems to be a natural choice to use a boundary integral equation approach for the approximate solution of the forward problem [18, 19], for finite element methods, see, e.g., [11, 15, 23].

This paper is organised as follows: In Sect. 2 we describe the mathematical model of the forward problem, i.e. the material parameters and the modelling of the excitation coils, and we discuss the eddy current model and a reduced simplified model. Bounds for the approximation error of certain quantities computed with the reduced and the eddy current model are presented in Sect. 3. In Sect. 4, a boundary element formulation for the reduced model is given, and some numerical results in Sect. 5 conclude the paper.

2 Eddy current model

In this section we formulate the forward problem of magnetic induction tomography (MIT) by using the eddy current formulation. The use of the eddy current model is justified since the wavelength for operating frequencies of MIT systems, which lie typically between 10 MHz and 100 MHz, is in the range of some micrometers, so the wavelength is small compared to the size of the conductor.

Let $\Omega \subset \mathbb{R}^3$ be a bounded domain, which represents the conducting object, and let $\Omega^c = \mathbb{R}^3 \setminus \overline{\Omega}$ be the exterior domain, where we assume a non-conducting material, e.g., air. For $x \in \Omega^c$ we therefore assume $\sigma(x) = 0$. The eddy current model of magnetic induction tomography is obtained by neglecting the displacement currents \mathbf{D} in the non-conducting material domain Ω^c , i.e. we set $\varepsilon(x) = 0$ for $x \in \Omega^c$. Hence we can rewrite the partial differential equation (1.2) as a system of two coupled equations,

$$\nabla \times \frac{1}{\mu_0} \nabla \times \mathbf{E}(x) + i\omega\kappa(x)\mathbf{E}(x) = -i\omega\mathbf{j}_i(x), \quad \nabla \cdot [\varepsilon(x)\mathbf{E}(x)] = 0 \quad \text{for } x \in \Omega, \quad (2.1)$$

and

$$\nabla \times \frac{1}{\mu_0} \nabla \times \mathbf{E}(x) = -i\omega\mathbf{j}_i(x) \quad \text{for } x \in \Omega^c, \quad (2.2)$$

where we introduce the gauging condition

$$\nabla \cdot \mathbf{E}(x) = 0 \quad \text{for } x \in \Omega^c. \quad (2.3)$$

In addition we assume radiation conditions at infinity, i.e.,

$$\mathbf{E}(x) = \mathcal{O}(|x|^{-1}), \quad \nabla \times \mathbf{E}(x) = \mathcal{O}(|x|^{-2}) \quad \text{as } |x| \rightarrow \infty. \quad (2.4)$$

Moreover, we have to include transmission boundary conditions for $x \in \Gamma = \partial\Omega$,

$$[\mathbf{j}(x) \cdot \mathbf{n}_x]_{|x \in \Gamma} = 0, \quad [\mathbf{H}(x) \times \mathbf{n}_x]_{|x \in \Gamma} = 0,$$

which can be rewritten as

$$[\kappa(x)\mathbf{E}(x) \cdot \mathbf{n}_x]_{|x \in \Gamma} = 0, \quad \frac{1}{i\omega\mu_0} [(\nabla \times \mathbf{E}(x)) \times \mathbf{n}_x]_{|x \in \Gamma} = 0. \quad (2.5)$$

Note that the jump is given by

$$[v(x)]_{|x \in \Gamma} = \lim_{\Omega^c \ni \tilde{x} \rightarrow x \in \Gamma} v(\tilde{x}) - \lim_{\Omega \ni \bar{x} \rightarrow x \in \Gamma} v(\bar{x}).$$

For the solution of the transmission problem (2.1)–(2.5) we introduce the decomposition

$$\mathbf{E}(x) = \mathbf{E}_s(x) + \mathbf{E}_p(x), \quad (2.6)$$

where \mathbf{E}_p denotes the primary field generated by the exciting coil \mathcal{C} without the presence of a conducting object. Correspondingly, \mathbf{E}_s is the secondary or reaction field caused by the presence of some conducting material. In particular, the primary field \mathbf{E}_p is a solution of the partial differential equations

$$\nabla \times \nabla \times \mathbf{E}_p(x) = -i\omega\mu_0\mathbf{j}_i(x), \quad \nabla \cdot \mathbf{E}_p(x) = 0 \quad \text{for } x \in \mathbb{R}^3,$$

which can be written as

$$-\Delta \mathbf{E}_p(x) = -i\omega\mu_0\mathbf{j}_i(x) \quad \text{for } x \in \mathbb{R}^3.$$

Hence we obtain a particular solution by the Newton potential

$$\mathbf{E}_p(x) = -i\omega\mu_0 \frac{1}{4\pi} \int_{\mathbb{R}^3} \frac{\mathbf{j}_i(y)}{|x-y|} dy \quad \text{for } x \in \mathbb{R}^3. \quad (2.7)$$

Hence, instead of (2.1) and (2.2) it remains to solve the following system of partial differential equations, i.e., for $x \in \Omega$

$$\nabla \times \frac{1}{\mu_0} \nabla \times \mathbf{E}_s(x) + i\omega\kappa(x)\mathbf{E}_s(x) = -i\omega\kappa(x)\mathbf{E}_p(x), \quad \nabla \cdot [\varepsilon(x)(\mathbf{E}_s(x) + \mathbf{E}_p(x))] = 0, \quad (2.8)$$

and

$$\nabla \times \nabla \times \mathbf{E}_s(x) = 0, \quad \nabla \cdot \mathbf{E}_s(x) = 0 \quad \text{for } x \in \Omega^c, \quad (2.9)$$

and with the radiation conditions

$$\mathbf{E}_s(x) = \mathcal{O}(|x|^{-1}), \quad \nabla \times \mathbf{E}_s(x) = \mathcal{O}(|x|^{-2}) \quad \text{as } |x| \rightarrow \infty. \quad (2.10)$$

If we define

$$\mathbf{H}(\text{curl}; \mathbb{R}^3) := \{ \mathbf{U} \in L_2(\mathbb{R}^3), \nabla \times \mathbf{U} \in L_2(\mathbb{R}^3) \},$$

the variational formulation of the transmission problem (2.8), (2.9), and (2.10) reads to find $\mathbf{E}_s \in \mathbf{H}(\text{curl}; \mathbb{R}^3)$ such that

$$\frac{1}{\mu_0} \int_{\mathbb{R}^3} (\nabla \times \mathbf{E}_s(x)) \cdot (\nabla \times \overline{\mathbf{F}(x)}) dx + i\omega \int_{\Omega} \kappa(x) \mathbf{E}_s(x) \cdot \overline{\mathbf{F}(x)} dx = -i\omega \int_{\Omega} \kappa(x) \mathbf{E}_p(x) \cdot \overline{\mathbf{F}(x)} dx \quad (2.11)$$

is satisfied for all $\mathbf{F} \in \mathbf{H}(\text{curl}; \mathbb{R}^3)$. The null space of the variational problem (2.11) can be characterised by the function $\mathbf{E}_\varphi(x) = 0$ for $x \in \Omega$ and $\mathbf{E}_\varphi(x) = \nabla\varphi(x)$ for $x \in \Omega^c$, where φ is the unique solution of the exterior Dirichlet boundary value problem

$$-\Delta\varphi(x) = 0 \quad \text{for } x \in \Omega^c, \quad \varphi(x) = 1 \quad \text{for } x \in \Gamma, \quad \varphi(x) = \mathcal{O}(|x|^{-1}) \quad \text{as } |x| \rightarrow \infty.$$

We assume that the boundary $\Gamma = \partial\Omega$ has only one connected component. The variational formulation (2.11) of the transmission problem (2.8)–(2.10) is therefore not uniquely solvable. Hence we introduce the gauging condition

$$\int_{\Gamma} \mathbf{E}(x) \cdot \mathbf{n}_x ds_x = 0, \quad (2.12)$$

which corresponds to the conservation of charge. We define

$$\mathcal{V} = \left\{ \mathbf{E} \in \mathbf{H}(\text{curl}, \mathbb{R}^3) : \text{div}\mathbf{E}(x) = 0 \quad \text{for } x \in \Omega^c, \int_{\Gamma} \mathbf{E}(x) \cdot \mathbf{n}_x ds_x = 0 \right\}.$$

The variational problem (2.11) then admits a unique solution $\mathbf{E}_s \in \mathcal{V}$, see [1, 3].

3 A reduced model

The solution of the forward problem using the eddy current model as described in the previous section is computationally rather expensive. Since in most solution algorithms for the inverse problem the forward problem has to be solved quite often, we are interested in a simplified model which also allows a more efficient solution of the forward problem. For this we write the transmission problem (2.8)–(2.10) in terms of the \mathbf{A} – ϕ –formulation [2]. Since \mathbf{B} is divergence-free, we can represent the magnetic flux density \mathbf{B} as the curl of a magnetic vector potential \mathbf{A} ,

$$\mathbf{B}(x) = \mu_0 \mathbf{H}(x) = \text{curl} \mathbf{A}(x) \quad \text{for } x \in \mathbb{R}^3.$$

From

$$\text{curl} \mathbf{E}(x) = -i\omega \mu_0 \mathbf{H}(x) = -i\omega \text{curl} \mathbf{A}(x)$$

we conclude the existence of a scalar potential ϕ satisfying

$$\mathbf{E}(x) + i\omega \mathbf{A}(x) = -\nabla \phi(x) \quad \text{for } x \in \mathbb{R}^3,$$

where ϕ is uniquely determined by the Coulomb gauge

$$\text{div} \mathbf{A}(x) = 0 \quad \text{for } x \in \mathbb{R}^3. \quad (3.1)$$

By using the decomposition (2.6) we can write the primary field \mathbf{E}_p as

$$\mathbf{E}_p(x) = -i\omega \mathbf{A}_p(x) \quad \text{for } x \in \mathbb{R}^3,$$

while for the secondary field \mathbf{E}_s we obtain

$$\mathbf{E}_s(x) = -i\omega \mathbf{A}_s(x) - \nabla \phi(x) \quad \text{for } x \in \mathbb{R}^3.$$

Note that

$$\mathbf{A}_p(x) = \frac{\mu_0}{4\pi} \int_{\mathbb{R}^3} \frac{\mathbf{j}_i(y)}{|x-y|} dy \quad \text{for } x \in \mathbb{R}^3$$

is a solution of the partial differential equations

$$\nabla \times \frac{1}{\mu_0} \nabla \times \mathbf{A}_p(x) = \mathbf{j}_i(x), \quad \nabla \cdot \mathbf{A}_p(x) = 0 \quad \text{for } x \in \mathbb{R}^3. \quad (3.2)$$

Now we can rewrite the eddy current model (2.1)–(2.4) for $x \in \mathbb{R}^3$ as

$$\nabla \times \frac{1}{\mu_0} \nabla \times \mathbf{A}_s(x) + \kappa(x)[i\omega \mathbf{A}_s(x) + \nabla \phi(x)] = -i\omega \kappa(x) \mathbf{A}_p(x), \quad (3.3)$$

$$\nabla \cdot \mathbf{A}_s(x) = 0. \quad (3.4)$$

When applying the divergence operator to equation (3.3), this gives

$$-\nabla \cdot [\kappa(x)(i\omega \mathbf{A}_s(x) + \nabla \phi(x))] = i\omega \nabla \cdot [\kappa(x) \mathbf{A}_p(x)] \quad \text{for } x \in \Omega. \quad (3.5)$$

In addition, we rewrite the transmission boundary condition (2.5) in terms of \mathbf{A} and ϕ and obtain

$$\kappa(x)[i\omega(\mathbf{A}_s(x) + \mathbf{A}_p(x)) + \nabla\phi(x)] \cdot \mathbf{n}_x = 0 \quad \text{for } x \in \Gamma. \quad (3.6)$$

In the parameter range of magnetic induction tomography numerical examples [5] indicate that \mathbf{A}_s is very small compared to $\nabla\phi$. Therefore we neglect \mathbf{A}_s in (3.5) and (3.6), i.e. we finally conclude the Neumann boundary value problem

$$-\nabla \cdot [\kappa(x)\nabla\tilde{\phi}(x)] = i\omega \nabla \cdot [\kappa(x)\mathbf{A}_p(x)] \quad \text{for } x \in \Omega, \quad (3.7)$$

$$\kappa(x)\frac{\partial}{\partial n_x}\tilde{\phi}(x) = -i\omega\kappa(x)\mathbf{A}_p(x) \cdot \mathbf{n}_x \quad \text{for } x \in \Gamma, \quad (3.8)$$

where $\tilde{\phi}$ now denotes the potential in the reduced model. Since $\tilde{\phi}$ is not uniquely determined by the Neumann boundary value problem (3.7) and (3.8), we introduce the scaling condition

$$\int_{\Gamma} \tilde{\phi}(x) ds_x = 0. \quad (3.9)$$

Moreover, by neglecting \mathbf{A}_s in (3.3) we obtain

$$\nabla \times \frac{1}{\mu_0} \nabla \times \tilde{\mathbf{A}}_s(x) = -\kappa(x)[i\omega\mathbf{A}_p(x) + \nabla\tilde{\phi}(x)], \quad \nabla \cdot \tilde{\mathbf{A}}_s(x) = 0 \quad \text{for } x \in \mathbb{R}^3,$$

i.e.

$$-\Delta\tilde{\mathbf{A}}_s(x) = -\mu_0\kappa(x)[i\omega\mathbf{A}_p(x) + \nabla\tilde{\phi}(x)] \quad \text{for } x \in \mathbb{R}^3.$$

Hence we conclude

$$\tilde{\mathbf{A}}_s(x) = -\frac{\mu_0}{4\pi} \int_{\Omega} \kappa(y) \frac{i\omega\mathbf{A}_p(y) + \nabla\tilde{\phi}(y)}{|x-y|} dy \quad \text{for } x \in \mathbb{R}^3. \quad (3.10)$$

The electric field can finally be obtained by

$$\tilde{\mathbf{E}}_s(x) = -i\omega\tilde{\mathbf{A}}_s(x) - \nabla\tilde{\phi}(x) \quad \text{for } x \in \mathbb{R}^3. \quad (3.11)$$

This means that the solution of the full eddy current model reduces to the solution of a Neumann boundary value problem for the Laplace equation, and the evaluation of a Newton potential. Both models are summarised in Table 1.

It remains to estimate the error when considering the reduced model instead of the eddy current model, see also [17]. In particular we have to consider the differences $\phi - \tilde{\phi}$ and $\mathbf{A}_s - \tilde{\mathbf{A}}_s$, respectively. For this, we first introduce the Newton potential operator

$$(N_0 u)(x) = \frac{1}{4\pi} \int_{\Omega} \frac{u(y)}{|x-y|} dy \quad \text{for } x \in \Omega.$$

In the case of a vector-valued function \mathbf{u} we consider the Newton potential $N_0\mathbf{u}$ component-wise.

Reduced model
$\mathbf{A}_p(x) = \frac{\mu_0}{4\pi} \int_{\mathbb{R}^3} \frac{\mathbf{j}_i(y)}{ x-y } ds_y \quad \text{for } x \in \mathbb{R}^3,$ $-\nabla \cdot [\kappa(x) \nabla \tilde{\phi}(x)] = i\omega \nabla \cdot [\kappa(x) \mathbf{A}_p(x)] \quad \text{for } x \in \Omega,$ $\kappa(x) \frac{\partial}{\partial n_x} \tilde{\phi}(x) = -i\omega \kappa(x) \mathbf{A}_p(x) \cdot \mathbf{n}_x \quad \text{for } x \in \Gamma, \quad \int_{\Gamma} \tilde{\phi}(x) ds_x = 0,$ $\tilde{\mathbf{A}}_s(x) = -\frac{\mu_0}{4\pi} \int_{\Omega} \kappa(y) \frac{i\omega \mathbf{A}_p(y) + \nabla \tilde{\phi}(y)}{ x-y } dy \quad \text{for } x \in \mathbb{R}^3,$ $\tilde{\mathbf{E}}_s(x) = -i\omega \tilde{\mathbf{A}}_s(x) - \nabla \tilde{\phi}(x) \quad \text{for } x \in \mathbb{R}^3$
Eddy current model
$\mathbf{E}_p(x) = -i\omega \frac{\mu_0}{4\pi} \int_{\mathbb{R}^3} \frac{\mathbf{j}_i(y)}{ x-y } dy \quad \text{for } x \in \mathbb{R}^3,$ $\nabla \times \frac{1}{\mu_0} \nabla \times \mathbf{E}_s(x) + i\omega \kappa(x) \mathbf{E}_s(x) = -i\omega \kappa(x) \mathbf{E}_p(x) \quad \text{for } x \in \Omega,$ $\nabla \times \frac{1}{\mu_0} \nabla \times \mathbf{E}_s(x) = 0 \quad \text{for } x \in \Omega^c,$ $\nabla \cdot [\varepsilon(x) (\mathbf{E}_s(x) + \mathbf{E}_p(x))] = 0 \quad \text{for } x \in \Omega,$ $\nabla \cdot \mathbf{E}_s(x) = 0 \quad \text{for } x \in \Omega^c$

Table 1: Comparison of the reduced model and the eddy current model.

Lemma 3.1 *Assume $\Omega \subset B_r(0)$. The Newton potential operator $N_0 : L_2(\Omega) \rightarrow L_2(\Omega)$ is bounded satisfying*

$$\|N_0\| := \sup_{u \in L_2(\Omega)} \frac{\|N_0 u\|_{L_2(\Omega)}}{\|u\|_{L_2(\Omega)}} \leq \frac{r^2}{\sqrt{3}}.$$

Proof. By using the Hölder inequality we have

$$\|N_0 u\|_{L_2(\Omega)}^2 = \int_{\Omega} \left| \frac{1}{4\pi} \int_{\Omega} \frac{u(y)}{|x-y|} dy \right|^2 dx \leq \frac{1}{(4\pi)^2} \|u\|_{L_2(\Omega)}^2 \int_{\Omega} \int_{\Omega} \frac{1}{|x-y|^2} dy dx.$$

The assertion then follows from Schmidt's inequality, i.e.

$$\int_{\Omega} \frac{1}{|x-y|^2} dy \leq \int_{B_r(0)} \frac{1}{|x-y|^2} dy \leq 4\pi r \quad \text{for } x \in \mathbb{R}^3.$$

In particular we have

$$\int_{\Omega} \int_{\Omega} \frac{1}{|x-y|^2} dy dx \leq \int_{\Omega} 4\pi r dx \leq \int_{B_r(0)} 4\pi r dx = (4\pi)^2 \frac{r^4}{3},$$

which concludes the proof. \blacksquare

Let \mathbf{A}_s be the solution of the eddy current model (3.3)–(3.4), in particular by using (3.4) we can rewrite (3.3) as

$$-\Delta \mathbf{A}_s(x) = -\mu_0 \kappa(x) [i\omega \mathbf{A}_s(x) + i\omega \mathbf{A}_p(x) + \nabla \phi(x)] \quad \text{for } x \in \mathbb{R}^3. \quad (3.12)$$

Hence we can write \mathbf{A}_s as the Newton potential

$$\mathbf{A}_s(x) = -\mu_0 N_0(\kappa(i\omega \mathbf{A}_s + i\omega \mathbf{A}_p + \nabla \phi)). \quad (3.13)$$

Correspondingly, we have

$$\tilde{\mathbf{A}}_s(x) = -\mu_0 N_0(\kappa(i\omega \mathbf{A}_p + \nabla \tilde{\phi})) \quad (3.14)$$

where $\nabla \tilde{\phi}$ is chosen such that

$$\operatorname{div} \tilde{\mathbf{A}}_s(x) = 0 \quad \text{for } x \in \mathbb{R}^3. \quad (3.15)$$

We therefore conclude

$$\mathbf{A}_s - \tilde{\mathbf{A}}_s = -\mu_0 N_0(\kappa(i\omega \mathbf{A}_s + \nabla \phi^\delta)), \quad \phi^\delta := \phi - \tilde{\phi}. \quad (3.16)$$

Theorem 3.2 *Let us define*

$$\kappa_{\min} := \sqrt{\inf_{x \in \Omega} \Re(\kappa(x))^2 + \inf_{x \in \Omega} \Im(\kappa(x))^2}, \quad \kappa_{\max} := \sup_{x \in \Omega} |\kappa(x)|$$

and

$$q := \mu_0 \omega \kappa_{\max} \left(1 + \frac{\kappa_{\max}}{\kappa_{\min}} \right) \frac{r^2}{\sqrt{3}}.$$

Let $\phi, \tilde{\phi} \in H^1(\Omega)$ be the weak solutions of the Neumann type boundary value problems (3.5)–(3.6) and (3.7)–(3.8), respectively. Then there holds the error estimate

$$\|\nabla \phi^\delta\|_{L_2(\Omega)} \leq \frac{\kappa_{\max}}{\kappa_{\min}} \omega \|\mathbf{A}_s\|_{L_2(\Omega)}. \quad (3.17)$$

If we assume $q < 1$, then there holds

$$\|\mathbf{A}_s\|_{L_2(\Omega)} \leq \frac{q}{1-q} \|\mathbf{A}_p\|_{L_2(\Omega)}, \quad (3.18)$$

and

$$\|\mathbf{A}_s - \tilde{\mathbf{A}}_s\|_{L_2(\Omega)} \leq \frac{q^2}{1-q} \|\mathbf{A}_p\|_{L_2(\Omega)}. \quad (3.19)$$

Proof. From (3.5) and (3.7) we first conclude that $\phi^\delta := \phi - \tilde{\phi}$ is a solution of the partial differential equation

$$-\nabla \cdot [\kappa(x)\nabla\phi^\delta(x)] = i\omega\nabla \cdot [\kappa(x)\mathbf{A}_s(x)] \quad \text{for } x \in \Omega$$

with the Neumann boundary condition

$$\kappa(x) \left[\frac{\partial}{\partial n_x} \phi^\delta(x) + i\omega \mathbf{A}_s(x) \cdot n_x \right] = 0 \quad \text{for } x \in \Gamma.$$

Hence, for $\psi \in H^1(\Omega)$ the weak formulation of the above Neumann boundary value problem reads

$$\begin{aligned} \int_{\Omega} \kappa(x)\nabla\phi^\delta(x) \cdot \nabla\psi(x) dx &= i\omega \int_{\Omega} \nabla \cdot [\kappa(x)\mathbf{A}_s(x)]\psi(x)dx + \int_{\Gamma} \kappa(x)\frac{\partial}{\partial n_x}\phi^\delta(x)\psi(x)ds_x \\ &= \int_{\Gamma} \kappa(x) \left[i\omega \mathbf{A}_s(x) \cdot n_x + \frac{\partial}{\partial n_x}\phi^\delta(x) \right] \psi(x)ds_x - i\omega \int_{\Omega} \kappa(x)\mathbf{A}_s(x) \cdot \nabla\psi(x)dx \\ &= -i\omega \int_{\Omega} \kappa(x)\mathbf{A}_s(x) \cdot \nabla\psi(x)dx. \end{aligned}$$

For $\psi = \phi^\delta$ we therefore have

$$\int_{\Omega} \kappa(x)|\nabla\phi^\delta(x)|^2 dx = -i\omega \int_{\Omega} \kappa(x)\mathbf{A}_s(x) \cdot \nabla\phi^\delta(x)dx,$$

from which (3.17) follows, i.e.

$$\|\nabla\phi^\delta\|_{L_2(\omega)} \leq \frac{\kappa_{\max}}{\kappa_{\min}} \omega \|\mathbf{A}_s\|_{L_2(\Omega)}.$$

Moreover, with (3.13) and by using Lemma 3.1 we further have

$$\begin{aligned} \|\mathbf{A}_s\|_{L_2(\Omega)} &= \mu_0 \|N_0(\kappa(i\omega\mathbf{A}_s + i\omega\mathbf{A}_p + \nabla\phi))\|_{L_2(\Omega)} \\ &\leq \mu_0 \kappa_{\max} \frac{r^2}{\sqrt{3}} \|i\omega\mathbf{A}_s + i\omega\mathbf{A}_p + \nabla\phi\|_{L_2(\Omega)} \\ &\leq \mu_0 \kappa_{\max} \frac{r^2}{\sqrt{3}} [\omega (\|\mathbf{A}_s\|_{L_2(\Omega)} + \|\mathbf{A}_p\|_{L_2(\Omega)}) + \|\nabla\phi\|_{L_2(\Omega)}]. \end{aligned} \quad (3.20)$$

The variational formulation of the Robin type boundary value problem (3.5) and (3.6) reads, for $\psi \in H^1(\Omega)$,

$$\begin{aligned} &\int_{\Omega} \kappa(x)\nabla\phi(x) \cdot \nabla\psi(x)dx \\ &= i\omega \int_{\Omega} \nabla \cdot [\kappa(x)(\mathbf{A}_p(x) + \mathbf{A}_s(x))]\psi(x)dx + \int_{\Gamma} \kappa(x)\frac{\partial}{\partial n_x}\phi(x)\psi(x)ds_x \\ &= \int_{\Gamma} \kappa(x) \left[i\omega(\mathbf{A}_p(x) + \mathbf{A}_s(x)) \cdot n_x + \frac{\partial}{\partial n_x}\phi(x) \right] \psi(x)ds_x \\ &\quad - i\omega \int_{\Omega} \kappa(x)(\mathbf{A}_p(x) + \mathbf{A}_s(x)) \cdot \nabla\psi(x)dx \\ &= -i\omega \int_{\Omega} \kappa(x)(\mathbf{A}_p(x) + \mathbf{A}_s(x)) \cdot \nabla\psi(x)dx. \end{aligned}$$

For $\psi = \phi$ we therefore have

$$\int_{\Omega} \kappa(x) |\nabla \phi(x)|^2 dx = -i\omega \int_{\Omega} \kappa(x) (\mathbf{A}_p(x) + \mathbf{A}_s(x)) \cdot \nabla \phi(x) dx,$$

from which the estimate

$$\|\nabla \phi\|_{L_2(\Omega)} \leq \frac{\kappa_{\max}}{\kappa_{\min}} \omega \|\mathbf{A}_p + \mathbf{A}_s\|_{L_2(\Omega)}$$

follows. From (3.20) we therefore conclude

$$\|\mathbf{A}_s\|_{L_2(\Omega)} \leq \mu_0 \kappa_{\max} \frac{r^2}{\sqrt{3}} \omega \left(1 + \frac{\kappa_{\max}}{\kappa_{\min}} \right) (\|\mathbf{A}_s\|_{L_2(\Omega)} + \|\mathbf{A}_p\|_{L_2(\Omega)}),$$

which immediately results in the estimate (3.18) when we assume $q < 1$.

Finally, by using (3.16) and Lemma 3.1 we have

$$\begin{aligned} \|\mathbf{A}_s - \tilde{\mathbf{A}}_s\|_{L_2(\Omega)} &= \mu_0 \|N_0(\kappa(i\omega \mathbf{A}_s + \nabla \phi^\delta))\|_{L_2(\Omega)} \\ &\leq \mu_0 \frac{r^2}{\sqrt{3}} \|\kappa(i\omega \mathbf{A}_s + \nabla \phi^\delta)\|_{L_2(\Omega)} \\ &\leq \mu_0 \kappa_{\max} \frac{r^2}{\sqrt{3}} (\omega \|\mathbf{A}_s\|_{L_2(\Omega)} + \|\nabla \phi^\delta\|_{L_2(\Omega)}) \\ &\leq \mu_0 \kappa_{\max} \frac{r^2}{\sqrt{3}} \omega \left(1 + \frac{\kappa_{\max}}{\kappa_{\min}} \right) \|\mathbf{A}_s\|_{L_2(\Omega)} = q \|\mathbf{A}_s\|_{L_2(\Omega)} \end{aligned}$$

due to (3.17). Now, (3.19) follows from (3.18). ■

Remark 3.1 *As an example we may consider a test problem with the following parameters:*

$$0.1 \leq \kappa(x) \leq 1 \quad \text{for } x \in \Omega, \quad \Omega \subset B_{0.1}(0), \quad \omega = 10^5.$$

In this case, we have

$$q = 7.98 \cdot 10^{-3}, \quad \frac{q^2}{1-q} = 6.42 \cdot 10^{-5}, \quad \|\mathbf{A}_p\|_{L_2(\Omega)} \approx 3.609 \cdot 10^{-6},$$

where the last result was obtained by using some finite element discretization.

Corollary 3.3 *In addition we have an estimate for the error in an arbitrary point $x \in \mathbb{R}^3$*

$$|\mathbf{A}_s(x) - \tilde{\mathbf{A}}_s(x)| \leq \frac{q^2}{1-q} \|\mathbf{A}_p\|_{L_2(B_r(0))}. \quad (3.21)$$

Proof. By using (3.16) we have, for $x \in \Omega$,

$$\begin{aligned}
|\mathbf{A}_s(x) - \tilde{\mathbf{A}}_s(x)| &= \frac{\mu_0}{4\pi} \left| \int_{\Omega} \kappa(x) \frac{i\omega \mathbf{A}_s(y) + \nabla \phi^\delta(y)}{|x-y|} dy \right| \\
&\leq \frac{\mu_0}{4\pi} \|\kappa(i\omega \mathbf{A}_s + \nabla \phi^\delta)\|_{L_2(\Omega)} \left(\int_{\Omega} \frac{1}{|x-y|^2} dy \right)^{1/2} \\
&\leq \frac{\mu_0}{4\pi} \kappa_{\max} \sqrt{4\pi r} (\omega \|\mathbf{A}_s\|_{L_2(\Omega)} + \|\nabla \phi^\delta\|_{L_2(\Omega)}) \\
&\leq \frac{\mu_0}{4\pi} \kappa_{\max} \sqrt{4\pi r} \omega \left(1 + \frac{\kappa_{\max}}{\kappa_{\min}} \right) \|\mathbf{A}_s\|_{L_2(\Omega)} = \frac{\sqrt{12\pi r}}{4\pi r^2} q \|\mathbf{A}_s\|_{L_2(\Omega)}
\end{aligned}$$

■

The quantity, which is measured in magnetic induction tomography is the voltage in the receiver coil \mathcal{C} , i.e.,

$$V := \int_{\mathcal{C}} \mathbf{B}_s(x) \cdot n_x ds_x.$$

Hence we need to evaluate

$$\mathbf{B}_s(x) = \nabla \times \mathbf{A}_s(x) = \frac{\mu_0}{4\pi} \int_{\Omega} \kappa(y) \nabla_x \frac{1}{|x-y|} \times [i\omega \mathbf{A}_p(y) + \nabla_y \phi(y)] dy \quad \text{for } x \in \mathcal{C}. \quad (3.22)$$

By using integration by parts, and by using

$$\nabla_x \frac{1}{|x-y|} = -\nabla_y \frac{1}{|x-y|},$$

the volume integral in (3.22) can be reformulated as

$$\begin{aligned}
\mathbf{B}_s(x) &= \frac{\mu_0}{4\pi} \sum_{k=1}^N \kappa_k \left(i\omega \int_{\Omega_k} \nabla_x \frac{1}{|x-y|} \times \mathbf{A}_p(y) dy - \int_{\Omega_k} \nabla_y \frac{1}{|x-y|} \times \nabla_y \phi(y) dy \right) \\
&= \frac{\mu_0}{4\pi} \sum_{k=1}^N \kappa_k \left(i\omega \int_{\Omega_k} \nabla_x \frac{1}{|x-y|} \times \mathbf{A}_p(y) dy - \int_{\Gamma_k} \frac{\nabla_y \phi(y) \times n_y}{|x-y|} ds_y \right),
\end{aligned}$$

where $\nabla_y \phi(y) \times n_y$ for $y \in \Gamma_k$ denotes the surface curl of the function ϕ .

4 A boundary element method for the reduced model

In this section we derive a boundary element formulation for the reduced model as described in the previous section. The variational formulation of the Neumann boundary value problem (3.7), (3.8) and (3.9) is to find $\tilde{\phi} \in H^1(\Omega)$ such that

$$\int_{\Omega} \kappa(x) \nabla \tilde{\phi}(x) \cdot \nabla \psi(x) dx + \int_{\Gamma} \tilde{\phi}(x) ds_x \int_{\Gamma} \psi(x) ds_x = i\omega \int_{\Omega} \kappa(x) \mathbf{A}_p(x) \cdot \nabla \psi(x) dx \quad (4.1)$$

for all $\psi \in H^1(\Omega)$. For a piecewise constant conductivity $\kappa(x)$ we consider a non-overlapping domain decomposition

$$\bar{\Omega} = \bigcup_{k=1}^p \bar{\Omega}_k, \quad \Omega_k \cap \Omega_\ell = \emptyset \text{ for } k \neq \ell, \quad \Gamma_S = \bigcup_{k=1}^p \Gamma_k, \quad \Gamma_k = \partial\Omega_k, \quad \kappa(x) = \kappa_k \text{ for } x \in \Omega_k.$$

Instead of the global Neumann boundary value problem (3.7) and (3.8) we now consider the local boundary value problems, by using (3.2),

$$-\kappa_k \Delta \tilde{\phi}|_{\Omega_k} = 0 \quad \text{for } x \in \Omega_k, \quad \kappa_k \frac{\partial}{\partial n_k} \tilde{\phi}(x) = -i\omega \kappa_k \mathbf{A}_p(x) \cdot n_x \quad \text{for } x \in \Gamma_k \cap \Gamma, \quad (4.2)$$

together with the transmission boundary conditions, see (2.5),

$$\kappa_k \frac{\partial}{\partial n_k} \tilde{\phi}(x) + \kappa_\ell \frac{\partial}{\partial n_\ell} \tilde{\phi}(x) = -i\omega \kappa_k \mathbf{A}_p(x) \cdot n_k - i\omega \kappa_\ell \mathbf{A}_p(x) \cdot n_\ell \quad \text{for } x \in \Gamma_k \cap \Gamma_\ell.$$

Thus we can rewrite the variational formulation (4.1) as

$$\sum_{k=1}^p \int_{\Gamma_k} \kappa_k \frac{\partial}{\partial n_k} \tilde{\phi}(x) \psi(x) ds_x + \int_{\Gamma} \tilde{\phi}(x) ds_x \int_{\Gamma} \psi(x) ds_x = - \sum_{k=1}^p i\omega \int_{\Gamma_k} \kappa_k [\mathbf{A}_p(x) \cdot n_k] \psi(x) ds_x.$$

For the solution of the local partial differential equation in (4.2) we use the local Dirichlet to Neumann map

$$\frac{\partial}{\partial n_x} \tilde{\phi}(x) = (S_k \tilde{\phi})(x) \quad \text{for } x \in \Gamma_k = \partial\Omega_k,$$

where $S_k : H^{1/2}(\Gamma_k) \rightarrow H^{-1/2}(\Gamma_k)$ is the associated Steklov–Poincaré operator [21]. Let $H^{1/2}(\Gamma_S) := H^1(\Omega)|_{\Gamma_S}$ be the skeleton trace space of $H^1(\Omega)$. We then have to solve a variational problem to find $\tilde{\phi} \in H^{1/2}(\Gamma_S)$ such that

$$\sum_{k=1}^p \kappa_k \int_{\Gamma_k} (S_k \tilde{\phi})(x) \psi(x) ds_x + \int_{\Gamma} \tilde{\phi}(x) ds_x \int_{\Gamma} \psi(x) ds_x = - \sum_{k=1}^p i\omega \int_{\Gamma_k} \kappa_k [\mathbf{A}_p(x) \cdot n_k] \psi(x) ds_x \quad (4.3)$$

is satisfied for all $\psi \in H^{1/2}(\Gamma)$. Since the bilinear form in the variational formulation (4.3) is bounded and $H^{1/2}(\Gamma_S)$ -elliptic, see, e.g. [12], unique solvability of the variational formulation (4.3) follows.

To describe the application of the local Steklov–Poincaré operators which are involved in the variational formulation (4.3) we use the symmetric boundary integral operator representations

$$(S_k \tilde{\phi}|_{\Gamma_k})(x) = \left[D_k + \left(\frac{1}{2}I + K'_k \right) V_k^{-1} \left(\frac{1}{2}I + K_k \right) \right] \tilde{\phi}|_{\Gamma_k}(x) \quad \text{for } x \in \Gamma, \quad (4.4)$$

where

$$(V_k w)(x) = \frac{1}{4\pi} \int_{\Gamma_k} \frac{1}{|x-y|} w(y) ds_y \quad \text{for } x \in \Gamma_k$$

is the single layer integral operator,

$$(K_k v)(x) = \frac{1}{4\pi} \int_{\Gamma_k} \frac{\partial}{\partial n_y} \frac{1}{|x-y|} v(y) ds_y \quad \text{for } x \in \Gamma_k$$

is the double layer integral operator, and

$$(D_k v)(x) = -\frac{1}{4\pi} \frac{\partial}{\partial n_x} \int_{\Gamma_k} \frac{\partial}{\partial n_y} \frac{1}{|x-y|} v(y) ds_y \quad \text{for } x \in \Gamma_k$$

is the so-called hypersingular boundary integral operator. The mapping properties of all boundary integral operators and therefore of the local Steklov–Poincaré operators S_k are well known, see, e.g. [4, 13, 14, 22].

For a symmetric boundary element discretization of the variational formulation (4.3) we introduce a sequence of admissible boundary element meshes $\Gamma_{S,h}$ with a globally quasi uniform mesh size h . Let $S_h^1(\Gamma_S)$ be the associated boundary element space of piecewise linear continuous basis functions φ_i . By $S_h^1(\Gamma_k) = S_h^1(\Gamma_S)|_{\Gamma_k}$ we denote the localised boundary element space of local basis functions $\varphi_{k,i}$, and by $\underline{\phi}_k = A_k \underline{\phi}$ we describe the localisation of the global degrees of freedom. The symmetric boundary element approximation of the variational problem (4.3) results in the linear system, see, e.g. [21],

$$\sum_{k=1}^p \kappa_k A_k^\top S_{k,h} A_k \underline{\phi} = -i\omega \sum_{k=1}^p \kappa_k A_k^\top \underline{f}_k, \quad (4.5)$$

where

$$S_{k,h} = D_{k,h} + \left(\frac{1}{2} M_{k,h}^\top + K_{k,h}^\top\right) V_{k,h}^{-1} \left(\frac{1}{2} M_{k,h} + K_{k,h}\right)$$

are the discrete Steklov–Poincaré operators. Note that

$$\begin{aligned} D_{k,h}[j, i] &= \langle D_k \varphi_{k,i}, \varphi_{k,j} \rangle_{\Gamma_k}, \\ V_{k,h}[\ell, m] &= \langle V_k \psi_{k,m}, \psi_{k,\ell} \rangle_{\Gamma_k}, \\ K_{k,h}[\ell, i] &= \langle K_k \varphi_{k,i}, \psi_{k,\ell} \rangle_{\Gamma_k}, \\ M_{k,h}[\ell, i] &= \langle \varphi_{k,i}, \psi_{k,\ell} \rangle_{\Gamma_k} \end{aligned}$$

are local boundary element matrices, and $S_h^0(\Gamma_k)$ are local boundary element spaces of, e.g., piecewise constant basis functions $\psi_{k,\ell}$. Moreover, the right hand side in (4.5) is given locally as

$$f_{k,j} = \int_{\Gamma_k} [\mathbf{A}_k(x) \cdot \mathbf{n}_k] \varphi_{k,j}(x) ds_x.$$

The stability and error analysis of the symmetric boundary element discretization of the variational problem (4.3) is well established, see, e.g. [21], and the references given therein.

5 Numerical results

As conducting domain we first consider the cylinder

$$\Omega = \{x \in \mathbb{R}^3, x_1^2 + x_2^2 < 0.1, 0 < x_3 < 0.2\},$$

where the transmitting coil is modelled as a current loop of radius 0.04 which is centred at $(-0.14, 0, 0.1)^\top$, see Fig. 2. The vector normal to the current loop points into the direction of the x_1 -axis, i.e., $n_x = (1, 0, 0)^\top$. Inside the cylinder we place a ball with radius $r = 0.02$, whose centre lies in the point $(-0.06, 0, 0.1)^\top$.

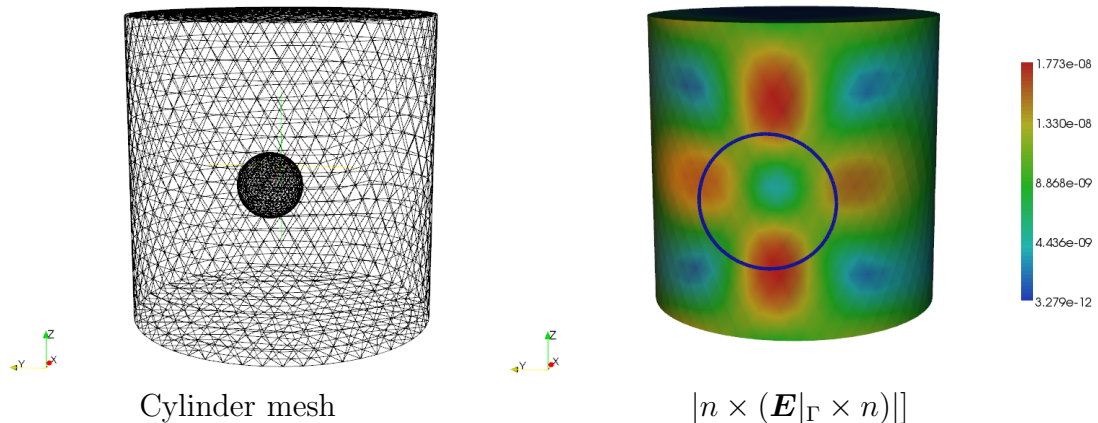


Figure 2: Mesh of the cylinder and the magnitude of the tangential electric field on Γ .

The background conductivity of the cylinder is $\kappa = 0.1$, and the conductivity of the inscribed ball is κ_{inc} . Fig. 2 shows the magnitude of the electric field $|n \times (\mathbf{E}|_\Gamma \times n)|$ for $\kappa_{\text{inc}} = 0.1$. In Fig. 3 we give a comparison of the reduced model with the full eddy current model. For this we plot the real and imaginary part of the normal component of the magnetic field $\mathbf{B}(x) \cdot n_x$ along a circle around the cylinder for the frequency $f = 100\text{kHz}$, and for varying conductivities $\kappa_{\text{inc}} \in \{0.1, 1, 10\}$. For the reduced model $\mathbf{B}(x) \cdot n_x$ was computed by using the boundary element approach as described in the previous section. The solution of the full eddy current problem was computed by using the Finite Element software packages Netgen [20] and NGSolve¹.

For the reduced model we have $\Re(\mathbf{B}(x) \cdot n_x) = 0$, while for the full eddy current model $\Re(\mathbf{B}(x) \cdot n_x)$ is comparable small. For the imaginary part we obtain a very good coincidence between the solution of the reduced and of the full model. Indeed, in Fig. 4 we give a plot of the error and of the relative error in $x = (-0.141, -0.141, 0.15)^\top$ between the normal magnetic field computed with the full eddy current model and the reduced model in the case $\kappa_{\text{inc}} = 0.1$, and for a frequency range from 100kHz up to 1GHz.

Based on the above results we conclude that the reduced model describes an appropriate approximation of the full eddy current model as used in magnetic induction tomography models.

¹<http://www.hpfem.jku.at/ngsolve/>

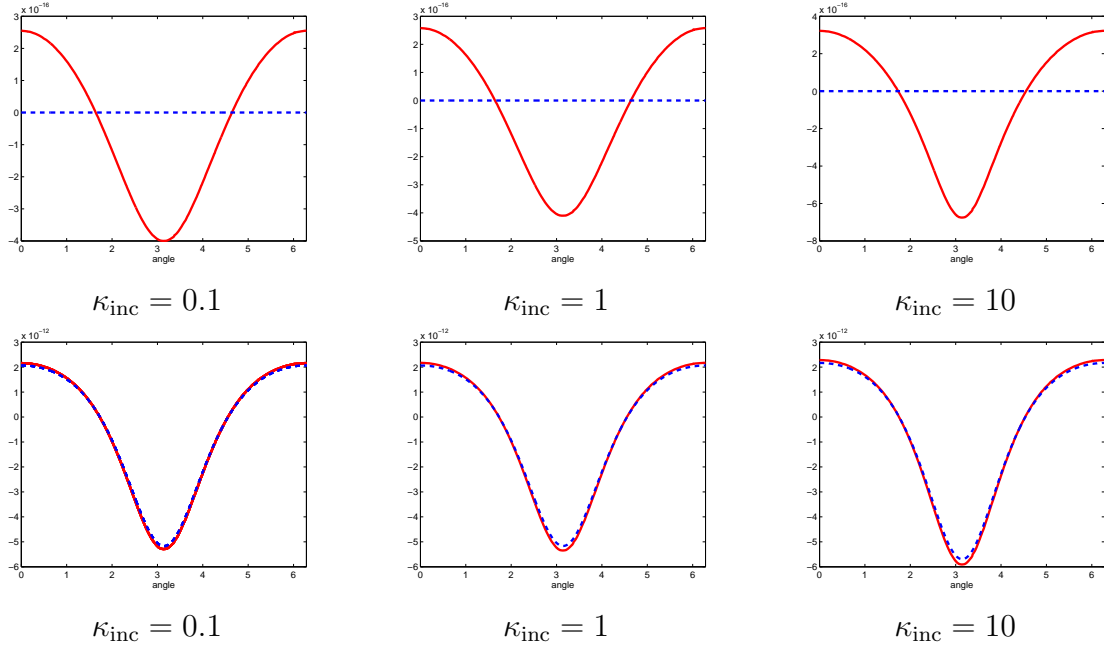


Figure 3: Real (upper row) and imaginary (lower row) parts of $\mathbf{B}(x) \cdot n_x$, $f = 10^5$.

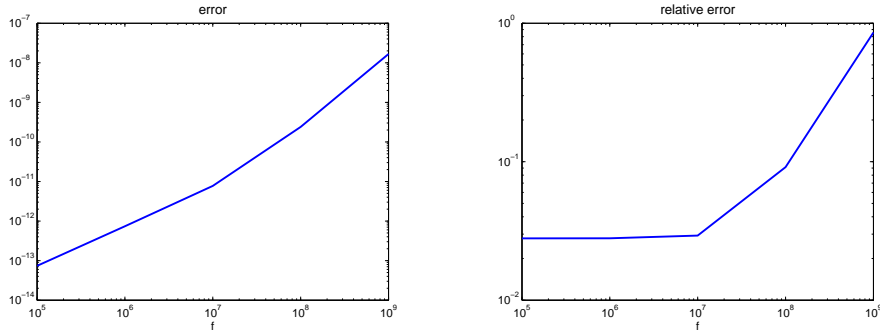


Figure 4: Absolute and relative point wise error for different frequencies.

In a second example we consider the model of a human thorax with two lungs, see Fig. 5. The volume mesh consists of 83514 volume elements and 15641 volume nodes, while the boundary element mesh consists of 13076 boundary elements and 7548 boundary nodes. The background conductivity of the thorax was set to the conductivity of a muscle at 100kHz, i.e., $\kappa_{\text{muscle}} = 0.3618\text{S/m}$, while the conductivity of the lungs is $\kappa_{\text{lung}} = 0.2716\text{S/m}$, see [8]. The centre of the transmitting coil was placed in the point $(0, -0.2, 0)^\top$, the normal vector of the coil is given by $(0, 1, 0)^\top$, and its radius is 0.05. In Fig. 5 we plot the magnitude of the tangential trace of the electric field, i.e. $|n \times (\mathbf{E}|_\Gamma \times n)|$. The field lines of the primary magnetic field \mathbf{B}_p of the secondary magnetic field \mathbf{B}_s are given in Fig. 6.

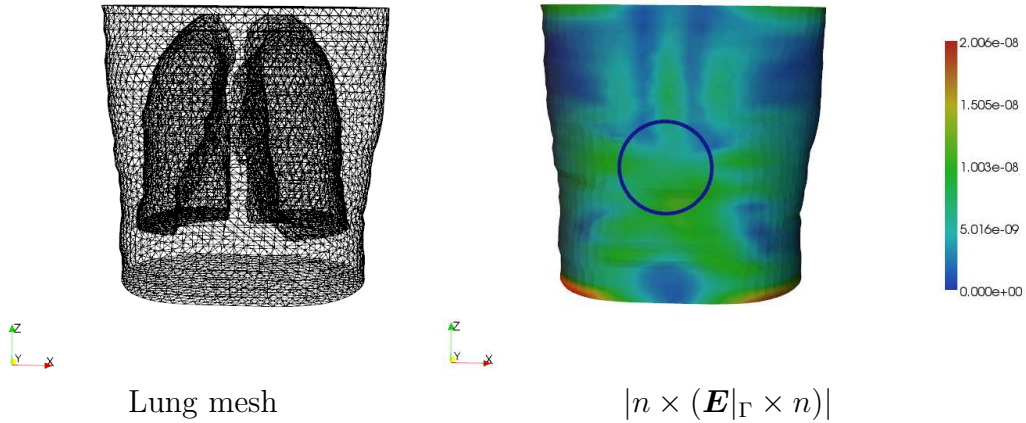


Figure 5: Mesh of the thorax and lungs and the magnitude of the tangential electric field.

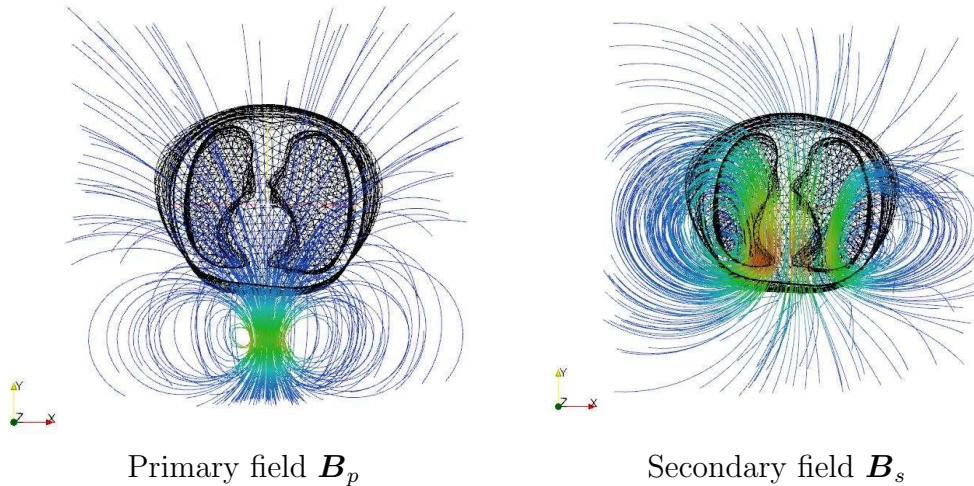


Figure 6: Field lines of the primary and secondary magnetic fields.

6 Conclusions and outlook

In this paper we derived two models which describe the forward problem of magnetic induction tomography, an eddy current problem and a reduced model. We proved estimates for the error between the reduced and the eddy current model, and we formulated a boundary element method for the reduced model. Numerical examples show that the reduced model is a good approximation for the eddy current model in the parameter range of magnetic induction tomography.

To be able to reconstruct the complex conductivity distribution inside the human body with magnetic induction tomography, an inverse problem has to be solved. For the reconstruction of the location and of the shape of organs, a shape reconstruction approach in

combination with a level set method can be used. For such an approach, the application of boundary element methods seems to be advantageous, since in every step of the level set method only the boundary has to be remeshed. The solution of the inverse problem demands a very fast solution of the forward problem on meshes with a high number of degrees of freedom. To establish a fast solver for the forward problem, fast boundary element methods may be employed such as the fast multipole method or hierarchical matrices.

Acknowledgement

This work has been supported by the Austrian Science Fund (FWF) under the grant SFB Mathematical Optimisation and Applications in Biomedical Sciences, Subproject Near Field Techniques for Biomedical Imaging. Furthermore we thank S. Zaglmayr for the help with the finite element computations. The authors also would like to thank H. Scharfetter and D. Gürsoy for many helpful discussions.

References

- [1] H. Ammari, A. Buffa, J.-C. Nédélec: A justification of eddy currents model for the Maxwell equations. *SIAM J. Appl. Math.* 60 (2000) 1805–1823.
- [2] O. Bíró: Edge element formulations of eddy current problems. *Comput. Methods Appl. Mech. Engrg.* 169 (1999) 391–405.
- [3] J. Breuer: Schnelle Randelementmethoden zur Simulation von elektrischen Wirbelstromfeldern sowie ihrer Wärmeproduktion und Kühlung. Dissertation, Universität Stuttgart, 2005.
- [4] M. Costabel: Boundary integral operators on Lipschitz domains: Elementary results. *SIAM J. Math. Anal.* 19 (1988) 613–626.
- [5] B. Dekdouk, W. Yin, C. Ktistis, D. W. Armitage, A. J. Peyton: A method to solve the forward problem in magnetic induction tomography based on the weakly coupled field approximation. *IEEE Trans. Biomed. Eng.* 54 () 914–921.
- [6] O. Dorn, H. Bertete–Aguirre, J. G. Berryman, G. C. Papanicolaou: A nonlinear inversion method for 3D electromagnetic imaging using adjoint fields. *Inverse Problems* 15 (1999) 1523–1558.
- [7] O. Dorn, U. Ascher: Shape reconstruction in 3D electromagnetic induction tomography using a level set technique. In: *Proceedings of the 23rd Review of Progress in Applied Computational Electromagnetics Conference ACES 2007, Verona, Italy*, pp. 695–700.

- [8] S. Gabriel, R. W. Lau, C. Gabriel: The dielectric properties of biological tissues: II. Measurements in the frequency range 10 Hz to 20 GHz. *Phys. Med. Biol.* 41 (1996) 2251–2269.
- [9] D. Gürsoy, H. Scharfetter: Optimum receiver array design for magnetic induction tomography. *IEEE Trans. Biomed. Eng.* 56 (2009) 1435–1441.
- [10] D. Gürsoy, H. Scharfetter: Reconstruction artefacts in magnetic induction tomography due to patient’s movement during data acquisition. *Physiol. Meas.* 30 (2009) 165–174.
- [11] C. Hollaus, K. Magele, R. Merwa, H. Scharfetter: Fast calculation of the sensitivity matrix in magnetic induction tomography by tetrahedral edge finite elements and the reciprocity theorem. *Physiol. Meas.* 25 (2004) 159–168.
- [12] G. C. Hsiao, O. Steinbach, W. L. Wendland: Domain decomposition methods via boundary integral equations. *J. Comput. Appl. Math.* 125 (2000) 521–537.
- [13] G. C. Hsiao, W. L. Wendland: *Boundary Integral Equations*. Springer, Heidelberg, 2008.
- [14] W. McLean: *Strongly Elliptic Systems and Boundary Integral Equations*. Cambridge University Press, 2000.
- [15] R. Merwa, K. Hollaus, B. Brandstätter, H. Scharfetter: Numerical solution of the general 3d eddy current problem for magnetic induction tomography. *Physiol. Meas.* 24 (2003) 545–554.
- [16] R. Merwa, K. Hollaus, P. Brunner, H. Scharfetter: Solution of the inverse problem of magnetic induction tomography. *Physiol. Meas.* 26 (2005) 241–250.
- [17] F. Natterer: An error bound for the Born approximation. *Inverse Problems* 20 (2004) 447–452.
- [18] M. H. Pham, A. J. Peyton: A model for the forward problem in magnetic induction tomography using boundary integral equations. *IEEE Trans. Magnet.* 44 (2008) 2262–2267.
- [19] M. H. Pham, A. J. Peyton: Computation of 3–d sensitivity coefficients in magnetic induction tomography using boundary integral equations and radial basis functions. *IEEE Trans. Magnet.* 44 (2008) 2268–2276.
- [20] J. Schöberl: Netgen an advancing front 2d/3d-mesh generator based on abstract rules. *Comput. Visual. Sci.* 1 (1997) 41–52.
- [21] O. Steinbach: Stability estimates for hybrid coupled domain decomposition methods. *Lecture Notes in Mathematics*, vol. 1809, Springer, Heidelberg, 2003.

- [22] O. Steinbach: Numerical approximation methods for elliptic boundary value problems. Finite and boundary elements. Springer, New York, 2008.
- [23] M. Zolgharni, P. D. Ledger, H. Griffiths: Forward modelling of magnetic induction tomography: a sensitivity study for detecting haemorrhagic cerebral stroke. *Med. Biol. Eng. Comput.* 47 (2009) 1301–1313.

Erschienene Preprints ab Nummer 2008/1

- 2008/1 P. Urthaler: Schnelle Auswertung von Volumenpotentialen in der Randelementmethode.
- 2008/2 O. Steinbach (ed.): Workshop on Numerical Simulation of the Maxwell Equations. Book of Abstracts.
- 2008/3 G. Of, O. Steinbach, P. Urthaler: Fast Evaluation of Newton Potentials in the Boundary Element Method.
- 2008/4 U. Langer, O. Steinbach, W. L. Wendland (eds.): 6th Workshop on Fast Boundary Element Methods in Industrial Applications, Book of Abstracts.
- 2008/5 D. Brunner, G. Of, M. Junge, O. Steinbach, L. Gaul: A Fast BE-FE Coupling Scheme for Partly Immersed Bodies
- 2009/3 G. Of, O. Steinbach: The All-Floating Boundary Element Tearing and Interconnecting Method.
- 2009/4 O. Steinbach: A note on the stable coupling of finite and boundary elements.
- 2009/5 O. Steinbach, M. Windisch: Stable boundary element domain decomposition methods for the Helmholtz equation.
- 2009/6 G. Of, W. L. Wendland, N. Zorii: On the Numerical Solution of Minimal Energy Problems.
- 2009/7 U. Langer, O. Steinbach, W. L. Wendland (eds.): 7th Workshop on Fast Boundary Element Methods in Industrial Applications, Book of Abstracts.
- 2009/8 H. Egger, M. Freiberger, M. Schlottbom: Analysis of Forward and Inverse Models in Fluorescence Optical Tomography.
- 2009/9 O. Steinbach, M. Windisch: Robust boundary element domain decomposition solvers in acoustics.
- 2009/10 M. Freiberger, H. Egger, H. Scharfetter: Nonlinear Inversion in Fluorescence Optical Tomography.
- 2009/11 H. Egger, M. Hanke, C. Schneider, J. Schöberl, S. Zaglmayr: Adjoint Sampling Methods for Electromagnetic Scattering.
- 2009/12 H. Egger, M. Schlottbom: Analysis and Regularization of Problems in Diffuse Optical Tomography.
- 2009/13 G. Of, T. X. Phan, O. Steinbach: An energy space finite element approach for elliptic Dirichlet boundary control problems.
- 2009/14 G. Of, O. Steinbach: Coupled FE/BE Formulations for the Fluid-Structure Interaction.
- 2010/1 G. Of, T. X. Phan, O. Steinbach: Boundary element methods for Dirichlet boundary control problems.
- 2010/2 P. D. Ledger, S. Zaglmayr: hp-Finite element simulation of three-dimensional eddy current problems on multiply connected domains.
- 2010/3 O. Steinbach, P. Urthaler: On the unique solvability of boundary integral equations in poroelasticity.